Available online at www.sciencedirect.com
SCIENCE DIRECT®
Acta Materialia 53 (2005) 477–485
Acta MATERIALIA
www.actamat-journals.com

Cracking and decohesion of a thin Al_2O_3 film on a ductile Al–5%Mg substrate

Changjin Xie, Wei Tong *

Department of Mechanical Engineering, Yale University, 219 Becton Center, 15 Prospect St., New Haven 06520-8284, Connecticut, USA

Received 23 March 2004; received in revised form 30 September 2004; accepted 2 October 2004

Abstract

A ductile metal substrate (1 mm thick Al–5%Mg) with a brittle thin film coating (0.1 μm thick Al_2O_3) was quasi-statically stretched to induce an array of parallel cracks in the coating. Additional cracking, decohesion, and buckling of the coating with increasing straining were observed using optical, scanning electron, and atomic force microscopes. The number of cracks per unit axial distance and the average opening gap of each crack were found to increase with increasing axial strain. A 2D finite element analysis incorporating a cohesive interface model of cracked coating segments was carried out to obtain both the normal stress distribution in coating segments with various widths and the shear stress distribution along coating–substrate interfaces. Both the fracture strength of the coating and the shear strength of the interface were estimated. Several theoretical analyses appeared in the literature on the cracking and decohesion of thin film coatings were critically discussed.

Keywords: Thin film coating; Atomic force microscopy; Tension test; Aluminum; Anodization

1. Introduction

Thin brittle films bonded to ductile substrates have diverse applications, such as in abrasion-resistant coatings, anti-corrosion protective coatings, and thermal barrier coatings [1–5]. In order to improve the mechanical reliability of these thin film coatings, the fracture and adhesion properties of the coatings are often of major consideration [6–21]. Various experimental methods such as the tensile test [2–4], four-point [6,9] or three-point [10] bend test, peel test [11], scratch test [10], and increasingly nanoindentation test [10,12–15] have been used to evaluate the coating fracture stress and interfacial strength between the coating and the substrate. For submicron thin film coatings, uniaxial tension of a flat coating–substrate coupon has been the method of choice in some recent investigations [16–20]. Besides only relatively simple and inexpensive testing instrumentation is needed, a tensile test produces in a well-controlled manner a large array of parallel cracks over the nominally homogenously deformed ductile substrate and it allows also in situ observation of cracking and decohesion of the coating via various microscopy tools.

Like any other type of mechanical tests, the interpretation of the tensile test data to extract intrinsic fracture and interfacial properties of the coating attached to a substrate is still non-trivial. Hu and Evans [6] obtained some analytical results on cracking and decohesion of thin film coatings on ductile substrates by assuming a sliding (yielding) interface and linearly elastic coating and substrate. Their results may thus not be applicable to the cases when the substrate is undergoing fully plastic deformation [16–20]. Agrawal and Raj [16] presented a theoretical analysis to estimate the ultimate shear strength of a metal–ceramic interface using the crack density or spacing data obtained from a tensile test.

* Corresponding author. Tel.: +1 203 432 4260; fax: +1 203 432 6775.
E-mail address: wei.tong@yale.edu (W. Tong).

1359-6454/$30.00
doi:10.1016/j.actamat.2004.10.005

They also concluded that the maximum and minimum crack spacing between the cracks should differ by a factor of two. However, their analysis was based on the assumption of a sinusoidal distribution of the interfacial shear stress and the validity of such an assumption has not been examined in details. Delannay and Warren [21] considered the possible effect of crack interactions and developed a statistical theory to relate the dependence of crack density on strain in terms of a flaw density distribution function. Jeong and Kwon [17] gave a detailed theoretical analysis based on shear lag approximation to estimate the fracture strain (and hence stress) from the minimum strain at which initial cracks developed and the interface shear strength from the external substrate strain and cracking spacing at the onset of saturation.

We present here both an experimental observation and a finite element stress analysis of cracked segments for an Al_2O_3/Al–5%Mg coating–substrate system. The objective of our study is to assess the sensitivity and limitation of the uniaxial tensile test for evaluating quantitatively both the coating fracture and interfacial failure properties of thin film coating–substrate systems. The interfacial decohesion process of the coating is simulated in the analysis using a cohesive zone interface model [22–24]. The theoretical analyses cited above will also be examined by comparing them against the experimental and numerical results obtained in our study. In Section 2, the tensile testing procedure and results for Al_2O_3/Al–5%Mg are first given. The finite element analysis and results are described in Section 3. Discussion and conclusions are offered in Section 4.

2. Experimental procedure and results

Uniaxial tensile testing of polycrystalline Al–5%Mg sheets with an anodic barrier type oxide coating was used in our study [18,19]. The gage section of the dog-bone shaped Al–5%Mg tensile test coupon had dimensions of 15 mm long, 3 mm wide and 1 mm thick while the thickness of the anodic oxide coating was only 0.1 μm. The metal substrate Al–5%Mg was first annealed at 400 °C for 2 h to obtain a completely recrystallized grain structure with an average grain size of 70 μm. After mechanical polishing and electropolishing, the Al–5%Mg test coupon was anodized in a solution of 3% tartaric acid while the current density and the applied voltage were controlled to ≈1 mA/cm^2 and 75 V, respectively [18]. The thickness of the anodic oxide coating is known to be a function of applied voltage at a rate of ≈14 Å per volt and can be increased only by increasing the applied voltage [1]. Consequently, a nonporous barrier type oxide coating of 0.1 μm was formed, covering completely one of the flat surfaces of the gage section of the Al–5%Mg test coupon.

Tensile testing of the Al–5%Mg flat sheet specimen was carried out quasi-statically on a desktop mini-tensile tester [25–27]. After each strain increment of about 1%, the test was interrupted and the tensile coupon was then digitally imaged by an atomic force microscope (Digital Instrument 3000) and then by an optical microscope for measuring the cracking and decohesion of the surface oxide coating. The tensile test coupon remained mounted and loaded in tension by the mini-tensile tester (i.e., only the screw driven cross-head was stopped temporarily) during image acquisition. The stress–strain curves of the 1 mm thick Al–5%Mg test coupons with and without a 0.1 μm Al_2O_3 oxide coating are indistinguishable within the experimental error levels [25,27] but some stress relaxation was observed when the test was interrupted. Extensive cracking of the oxide coating occurred during the tensile test. A regular array of long channel cracks more or less perpendicular to the axial loading direction appeared on the tensile coupon surface and the density of cracks increases with increasing straining. As shown in Fig. 1 the six images obtained by atomic force microscopy (AFM), the nucleation and growth of new cracks happened in a discrete manner in the middle of existing cracked coating segments and the cracks were deflected and sometimes even terminated at the surface grain boundary. Broadening of the existing cracks with increasing straining was also evident, indicating significant decohesion of the cracked coatings especially at large strains. At the later stage of the tensile test, buckling of the oxide coating occurred at locations when slip steps due to plastic deformation were formed on the Al–5%Mg surface along directions ≈45° inclined with the tensile loading direction. Extensive cracking and buckling of the oxide coating was also observed by scanning electron microscopy (SEM) at the end of the tensile test (at a final axial strain of about 20%). Buckling of the oxide coating did not occur everywhere as slip steps did not appear in all surface grains of the polycrystalline Al–5%Mg substrate [26].

Figs. 2 and 3 summarize the cracking and decohesion of the anodic oxide coating on Al–5%Mg in terms of the dependence of the average crack line spacing (the width of the cracked coating segments) and the average crack opening (the width of the exposed substrate at each channel crack) on the applied overall axial strain in the substrate. As shown in Fig. 2, the crack line spacing decreased quickly in the initial loading stage and then saturated gradually to final crack spacing. Broadening of the cracking lines (indicating the onset of interfacial failure of the coating) became more noticeable when cracking of the coating started to reach the saturation state. In summary, the cracking, decohesion, and buckling of the anodic oxide coating occurred sequentially during the initial, intermediate, and final stages of the tensile test.

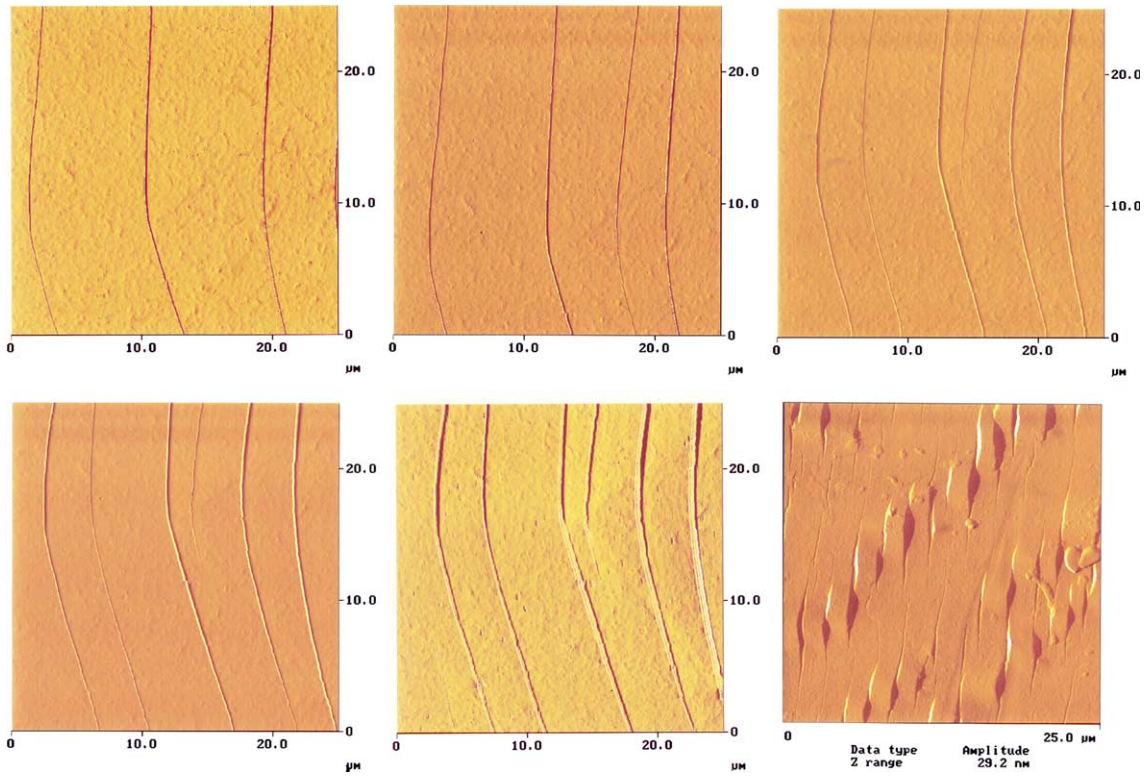

Fig. 1. Selected AFM images of the cracked oxide coating on Al_2O_3/Al–5%Mg. The images (from the upper left one to the lower right one) show the increasing density of coating cracks with increasing straining of the substrate and buckling of the oxide coating towards the end of tensile test. The tensile loading axis is aligned with the horizontal direction of the images. The deflection of cracks in the first five images occurred at the grain boundary due to heterogeneous plastic deformation occurred at the grain level [26,27]. Buckling of the oxide coating shown in the last image initiated at surface locations of slip bands.

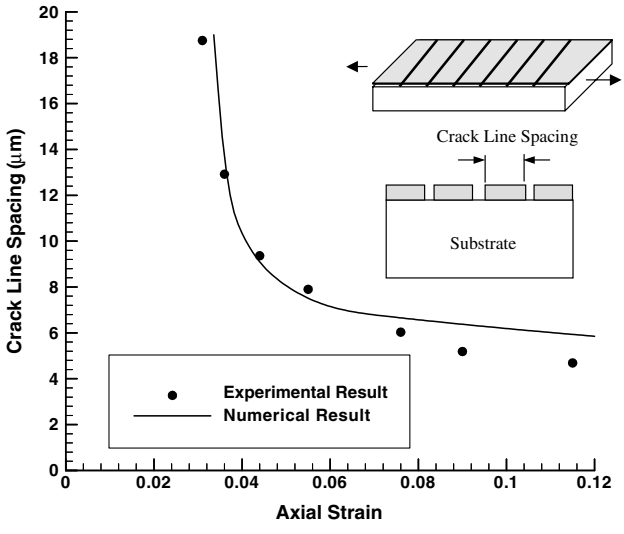

Fig. 2. Average crack line spacing vs. the overall axial strain of the substrate. Crack line spacing decreased quickly in the initial deformation stage and reached a saturation state after a strain of about 10%. Schematic of the cracked coating segments is also shown.

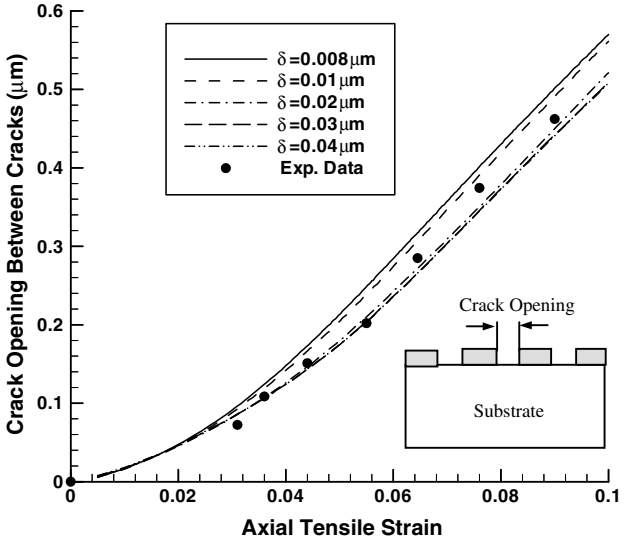

Fig. 3. Average crack opening between cracks vs. the overall axial strain of the substrate for different characteristic lengths (used in the cohesive interface model). Schematic of the cracked coating segments is also shown.

3. Numerical analysis of cracking and decohesion of oxide coatings

3.1. The finite element model of cracked coating segments

The objective of our numerical analysis was to characterize the stresses within the attached coating segments (see Fig. 4(a)). The analysis was carried out using the commercial nonlinear finite element code ABAQUS. However, as there is a very large mismatch between the dimensions of the thin film coating and those of the metal substrate (the ratio of the coating thickness over the substrate thickness is about 1:10,000 and the ratio of the cracked coating spacing over the gage length of the substrate is about 1:1000 or higher), it would be computationally inefficient if not impossible to analyze the entire geometry of the tensile specimen by the finite element method. A "unit cell" or single cracked segment attached to the substrate was analyzed instead by assuming the channel cracks are spaced more or less uniformly and perfectly aligned in parallel in the transverse direction of the test coupon. By the symmetry consideration, only half of a single cracked coating segment with a sufficient thick substrate part ABCDEF was modeled (see Fig. 4(a)). One needs to consider first how to impose the proper boundary conditions to this reduced problem. While it is straightforward to assign the boundary conditions for the symmetry plane ABC with all nodal displacements in the horizontal direction being set to zero but allow the nodes to move freely vertically (except one of the nodes such as at point C is fixed to a zero vertical displacement as well), the challenge is how to impose suitable boundary conditions along the boundary CF and the boundary EF for the reduced coating–substrate system shown in Fig. 4(a). The homogenous uniaxial tension boundary conditions for the whole test coupon at the far field may not be applicable to the boundaries CF and EF, respectively, of the reduced "unit cell" model. A series of finite element analyses were first performed on multiple coating segments (one, three, five, and seven, see Fig. 4(b)) to establish the proper depth of the substrate in the reduced coating–substrate model and to identify the suitable boundary conditions for CF and EF based on the St Venant's principle [19]. More specifically, both the depth of the substrate and the number of the coating segments were gradually increased until the convergence of the stress distribution in the coating and along the coating–substrate interface in the "unit cell" (the half of a coating segment at the left end) was reached. Our numerical simulations indicated that a reduced model with a substrate of at least 50 μm thick and up to five cracked coating segments were sufficiently accurate to capture the far-field uniaxial tension loading conditions of the substrate on the "unit cell" coating segment.

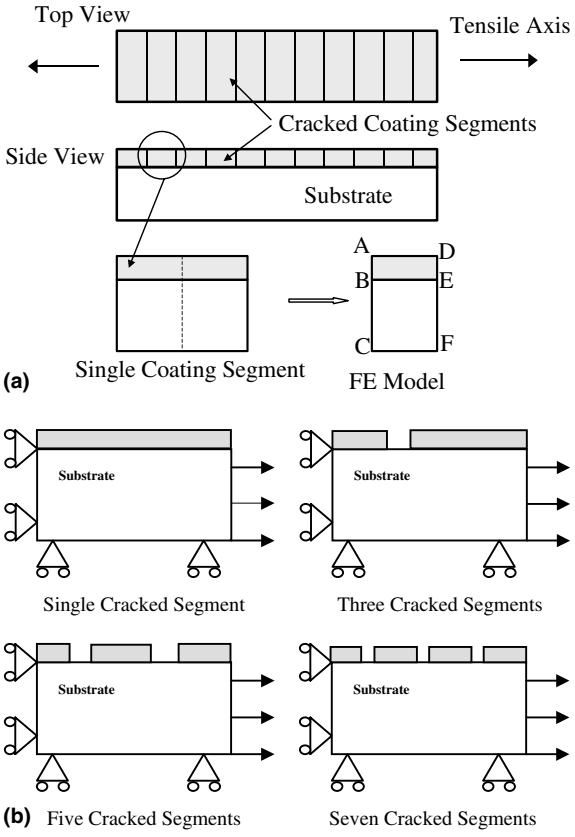

Fig. 4. (a) Schematic of the "unit cell" coating segment model ABCDEF used in the finite element analysis. ABC is the symmetry plane for the single coating segment and DE is the edge of a crack (completely running through the coating thickness). (b) A series of finite element models of the cracked coating segments for establishing the proper model size under far-field uniaxial tension. Due to the symmetry consideration, the convergence of the stress distributions in the coating and along the interface is examined for only half of the "unit cell" coating segment at the left end of each model in the numerical analysis.

Coating segments with different widths ranging from 20 to 4 μm were modeled using finite elements. Four-node, plane stress, reduced integration elements were used. The mesh density along the interface region and around the cracked edge (such as the regions along the interface BE and the DEF boundary shown in Fig. 4(a)) was increased in order to resolve the details of the plastic deformation and stress distribution in these places.

3.2. Coating and substrate material models

The thin film Al_2O_3 oxide coating was assumed to be linear isotropic elastic with a Young's modulus $E_c = 42$ GPa [3,5] and a Poisson's ratio $\nu_c = 0.25$ and that it fractures in a brittle manner at a certain fracture strain or fracture toughness. The substrate was modeled as an isotropic, rate-independent elastic–plastic solid with a Young's modulus $E_s = 70$ GPa and a Poisson's ratio $\nu_s = 0.3$. The von Mises effective true stress–strain curve

of the Al–5%Mg substrate [25,27] was approximated by the following equation:

$$\sigma = \sigma_Y + (\sigma_s - \sigma_Y)(1 - \exp(-\varepsilon/\varepsilon_s)), \quad (1)$$

where $\sigma_Y = 70$ MPa, $\sigma_s = 290$ MPa, and $\varepsilon_s = 0.1$ are, respectively, the yield strength, saturation flow stress and reference strain of the substrate.

3.3. Interfacial decohesion

Decohesion along the coating–substrate interface was simulated using a cohesive zone interface model [22–24]. In this model, the constitutive equation for the interface is prescribed such that, with increasing interfacial separation, the traction across the interface reaches a maximum, decreases, and eventually vanishes so that complete decohesion occurs in a gradual and controlled manner. Unlike the early work dealing with decohesion dominated by the normal traction and separation [22], decohesion of the oxide coating on a uniaxially strained substrate is dominated by the tangential traction and displacement. Similar to [24], the original interfacial cohesive zone model due to Needleman [22] was modified to model more effectively the shear-dominated decohesion of the oxide coating in the following.

An interface supporting a nominal traction field **T** (force/unit area) has both normal and tangential components. Two material points, P and Q, initially on opposite sides of the interface, are considered, and the interfacial traction is taken to depend only on the displacement difference across the interface, $\Delta\vec{u}_{PQ}$. At each point of the interface, we define normal and tangential displacements and tractions as

$$u_n = \vec{n} \cdot \Delta\vec{u}_{PQ}, \quad u_t = \vec{t} \cdot \Delta\vec{u}_{PQ} \quad (2)$$

and

$$T_n = \vec{n} \cdot \vec{T}, \quad T_t = \vec{t} \cdot \vec{T}. \quad (3)$$

In Eqs. (2) and (3), $\vec{n}, \vec{t}$ form a right-hand coordinate system chosen so that positive u_n corresponds to increasing separation and negative u_t corresponds to decreasing interfacial separation. The mechanical response of the interface is described through a constitutive relation that gives the dependence of the tractions T_n and T_t on u_n and u_t. Here, this response is specified in terms of a potential $\phi(u_n,u_t)$, where

$$\phi(u_n, u_t) = -\int_0^u [T_n \mathrm{d}u_n + T_t \mathrm{d}u_t]. \quad (4)$$

The specific potential function used is

$$\phi(u_n, u_t) = \frac{27}{4}\tau_{max}\delta\frac{\lambda^2}{2}\left(1 - \frac{4}{3}\lambda + \frac{1}{2}\lambda^2\right),$$
$$\lambda^2 = \left(\frac{u_t}{\delta}\right)^2 + \alpha\left(\frac{u_n}{\delta}\right)^2, \quad (5)$$

where τ_{max} is the maximum tangential traction per unit width that can be carried by the interface undergoing a purely shearing deformation (for $|u_t| \leqslant \delta$ and $u_n \equiv 0$), δ is a characteristic length in the tangential direction, and α specifies the coupling of normal to shear stiffness of the interface. The interfacial tractions are obtained by differentiating Eq. (5):

$$T_t = -\frac{\partial\phi}{\partial u_t} = -\frac{27\tau_{max}}{4}\frac{u_t}{\delta}\left(1 - 2\lambda + \lambda^2\right), \quad (6)$$

$$T_n = -\frac{\partial\phi}{\partial u_n} = -\frac{27\tau_{max}}{4}\alpha\frac{u_n}{\delta}\left(1 - 2\lambda + \lambda^2\right) \quad (7)$$

for $0 \leqslant \lambda \leqslant 1$, and $T_n \equiv T_t \equiv 0$ when $\lambda > 1$ ($u_n \geqslant 0$). The contact condition for normal compression ($u_n < 0$) of the interface may be approximately represented by elastic springs with high stiffness similar to [24] although it does not dominate in the substrate straining problem considered.

Prescription of three parameters τ_{max}, δ and α is required for the interface model given in Eq. (5). Values of these parameters were estimated by trial-and-error through a series of numerical simulations. Our simulation results show that both cracking and decohesion behaviors of the coating segments considered here were not very sensitive to the choice of α and so $\alpha = 1$ was thus used in all simulations reported in the following. As decohesion of the coating was clearly observed after 3–5% substrate strain, the maximum interfacial shear strength τ_{max} was reached during the test and it should be lower than or equal to the maximum shear flow stress of the substrate (i.e., the maximum shear stress can be exerted through the ductile substrate undergoing fully plastic deformation), which is about 150 MPa at 20% strain. By using τ_{max} somewhat smaller than 150 MPa and by requiring that decohesion of the coating at the crack edge be developed significantly after a few percent of plastic strain, τ_{max} was estimated to be ≈140 MPa. The characteristic length δ in the model was estimated by comparing the strain dependence of the average cracking opening from both experiments and simulations. As shown in Fig. 3, $\delta = 0.02$ μm gives the best match with the experimental data (using $\alpha = 1$, $\tau_{max} = 140$ MPa).

3.4. Finite element simulation results

Fig. 5(a) shows a typical axial tensile stress distribution in a coating segment (width = 19 μm). As expected, the in-plane tensile stress always reaches its maximum value at the middle point ($x = 0$ μm) of the coating segment and decreases rapidly to zero near the edge of the crack ($x = 9.5$ μm). Fig. 5(b) shows the shear stress distribution along the interface of the same coating segment. It shows that the shear stress develops gradually along the interface reaching its maximum near the crack.

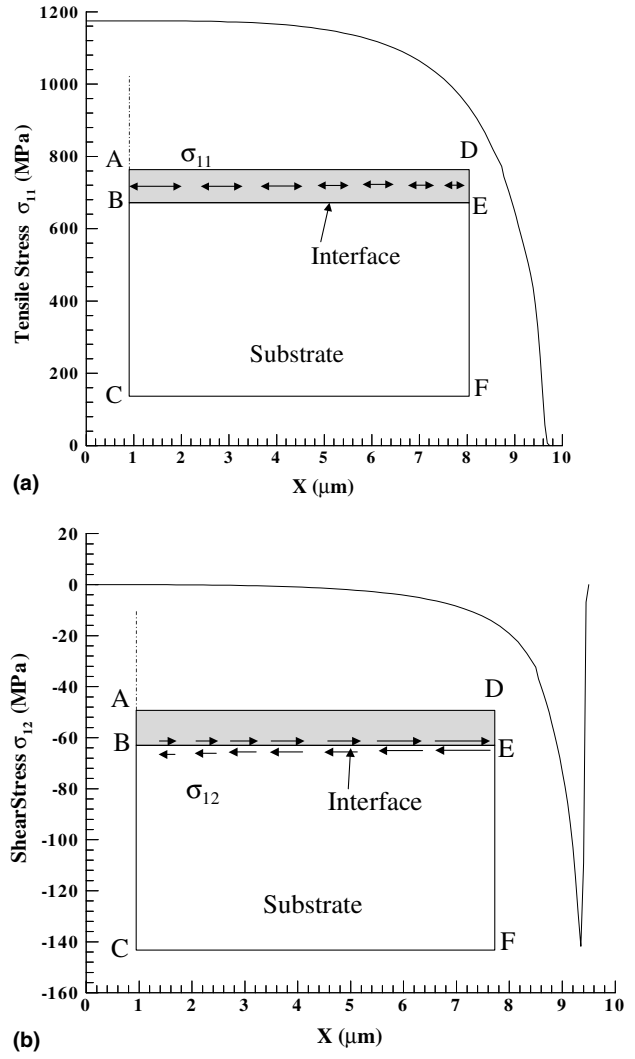

Fig. 5. (a) Normal tensile stress distribution within the coating; (b) shear stress distribution along the interface. The unit cell coating segment is 19 μm wide.

Some decohesion leads to its relaxation to zero towards the edge of the crack. The maximum shear stress level of 140 MPa is the same as the maximum interfacial shear strength prescribed for the interface model.

By performing a series of finite element analyses of cracked coating segments with various widths up to the strain levels observed in the experiment (see Fig. 2), the maximum tensile stress in the coating was found to be nearly identical, varying around the value of 1200 MPa. Alternatively, a series of finite element analyses were carried out for each coating segment width and the plastic strain levels were recorded when the maximum tensile stress in the coating reached 1200 MPa. Fig. 2 shows the comparison of the predicted (using the constant maximum tensile stress of 1200 MPa) and measured dependence of crack line spacing on the applied axial strain. An excellent fit up to the strain level of 7.6% is obtained. When the plastic deformation increases (beyond 7.6%), some extensive decohesion between the coating and substrate begins to occur in the numerical simulations, making the cracks line spacing much less dependent on further increasing strain. Nevertheless, the fracture strength (the stress level at which fracture occurs [28]) of this anodic oxide coating can be deduced to be about 1200 MPa. The excellent match with the experimental data on the dependence of crack line spacing on the applied axial strain shows that our finite element model can simulate the cracking behavior of this coating–substrate system reasonably well and one can indeed infer the coating fracture strength consistently.

By assuming different fracture strength for the coating, the sensitivity of the strain dependence of crack line spacing can be assessed. Fig. 6(a) shows the dependence of crack line spacings on the substrate

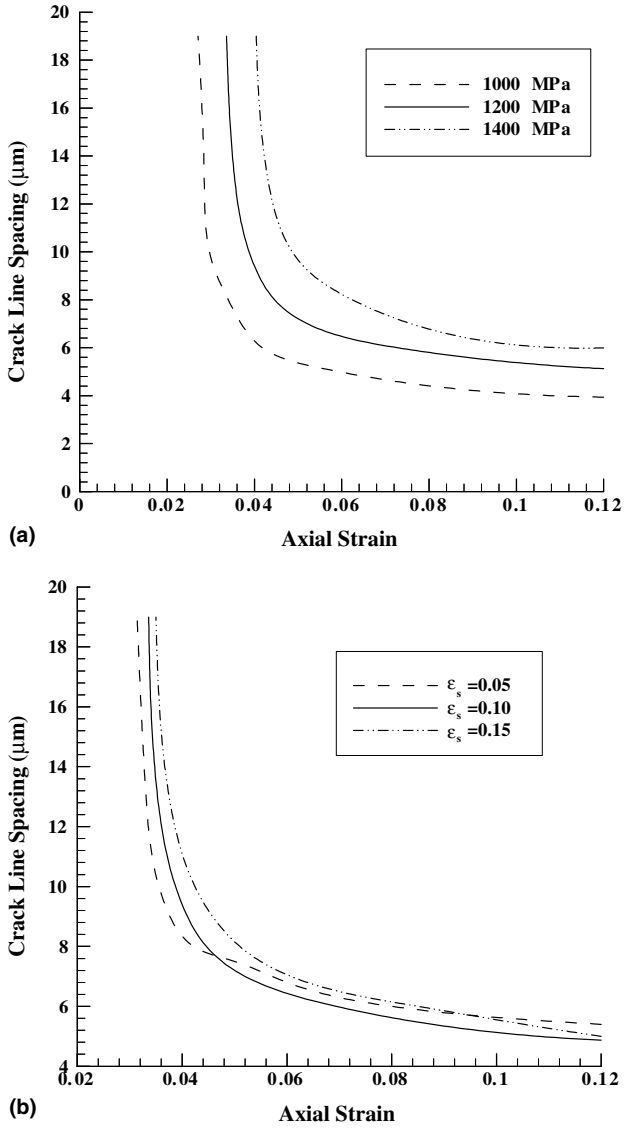

Fig. 6. Effects on the strain dependence of the crack line spacing of: (a) the maximum fracture strength of the coating; (b) strain hardening behavior of the substrate.

strain with respect to three different fracture strength levels of the coating (1000, 1200 and 1400 MPa). It turns out that the strain dependence of crack line spacing is rather sensitive to the coating fracture strength assumed. As expected, weaker coatings will fracture early and reach a lower saturated density of crack lines. Several other factors including strain hardening of the substrate, coating thickness, and the fracture criterion other than the maximum tensile stress that may affect the strain dependence of the cracking line spacing have also been examined. By varying the reference strain ε_s while keeping all other two parameters the same in Eq. (1), one can alter the strain hardening rate of the substrate. Fig. 6(b) shows the comparison of the strain dependence of crack line spacing assuming three different strain hardening behaviors with $\varepsilon_s = 0.05$, 0.1, 0.15 for the substrate (the fracture strength of 1200 MPa is assumed). Clearly, the substrate that strain hardens slowly ($\varepsilon_s = 0.15$) produces a more gradual transition towards the saturation.

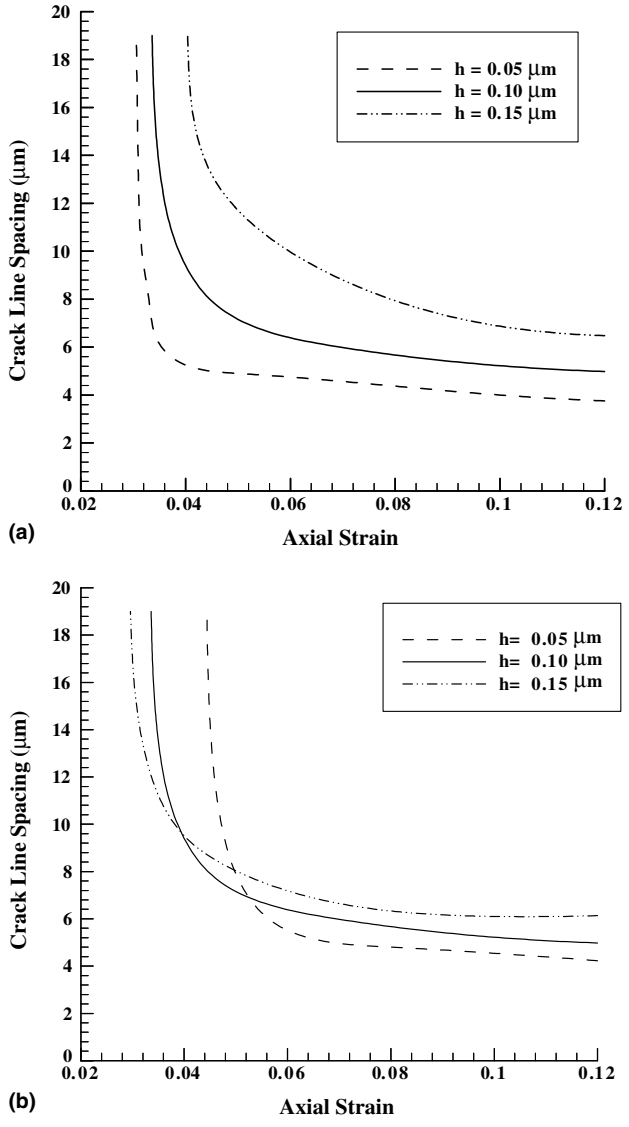

Fig. 7. The effect of the coating thickness on the strain dependence of crack line spacings: (a) the constant fracture stress criterion; (b) the constant fracture toughness criterion.

Fig. 7(a) shows the effect of the coating thickness ($h = 0.05$, 0.1, 0.15 μm) on the strain dependence of crack line spacing using the constant fracture stress criterion. It is seen that more plastic straining is needed to reach the saturation for thicker coatings but their steady-state crack line spacing is also larger. One can also replace the fracture stress criterion with a criterion based on the fracture toughness G_c, which has the following relation with the fracture strength σ_c and coating thickness h [29,30]

$$G_c \propto h\sigma_c^2. \tag{8}$$

Fig. 7(b) shows the effect of the coating thickness on the strain dependence of crack line spacing using the constant fracture toughness criterion, which is clearly different from that given in Fig. 7(a). In other words, one may be able to experimentally assess the most suitable criterion for predicting cracking in a given coating–substrate system by using coatings with various thicknesses.

4. Discussion and conclusions

When a ductile sheet metal Al–5%Mg substrate with a continuous anodic oxide film is subjected to uniaxial tension, the thin oxide film undergoes elastic deformation while the metal substrate undergoes elastic–plastic deformation. As the continuity between the thin film coating and the substrate must be maintained at their interface before failure, this gives rise to interfacial shear stress when the hard thin film, which shows little deformation, inhibits deformation of the substrate. As a result of the interfacial shear stress, force is transferred from the substrate to the thin film thus inducing the tensile stress in the thin film. As the substrate deformation increases, this tensile stress will accumulate and eventually reach the fracture strength of the coating. Parallel long cracks then shows up on the surface of the substrate with the thin film coating in a direction perpendicular to the tensile loading axis. Once the first array of multiple channel cracks are formed throughout the once continuous coating, the stresses within the cracked coating segments are relaxed and modified by the free edges of cracks and the coating deformation becomes nonhomogenous and far different from the overall uniform plastic deformation of the substrate. In this study, additional cracking of the fragmented coating and decohesion at the coating–substrate interface upon further straining of the substrate has been investigated by a simplified 2D finite element analysis incorporating a cohesive interface model. By matching the strain

dependence of the average crack line spacing and the average crack opening gap observed in the experiment, both the fracture strength of the coating and the shear strength of the coating–substrate interface have been estimated to be about 1200 and 140 MPa, respectively. The complicated coating buckling behavior [31,32] at large strains due to lateral contraction under uniaxial tension (see Fig. 1) has been omitted here.

As shown in Fig. 2, the minimal axial strain level in the substrate is about 3% when the channel cracks begin to emerge. Assuming that the strain in the *continuous* film is the same as the strain in the substrate, the fracture strength due to linear elasticity is $\sigma_c = E_f\varepsilon_c \approx 1260$ MPa, consistently with the above result. On the other hand, the shear strength of the interface $\hat{\tau}$ has been related to the film stress via [16,33–35]

$$\hat{\tau} = \frac{\pi h \sigma_c}{w_s}, \tag{9}$$

where w_s is the maximum spacing of the cracks when the crack density becomes constant. Using $h = 0.1$ μm and $w_s \approx 6$ μm, one obtains $\hat{\tau} \approx 63$ MPa, which is much less than our finite element analysis result. As shown in Fig. 5(b), the shear stress distribution along the interface of a cracked coating segment obtained in our analysis is not sinusoidal at all as previously suggested by Agrawal and Raj [16]. Consequently, their method of measuring the ultimate shear strength of a metal–ceramic interface may be quite inaccurate. The ultimate shear strength of the silica films on annealed 99.9% pure copper and nickel substrates was estimated to be 900 and 1400 MPa, respectively, by Agrawal and Raj [16,33]. However, these numbers are questionable as they greatly exceed the *shear* flow strength level for both metal substrates (assuming von Mises isotropic plasticity, the shear stress is only $1/\sqrt{3}$ of the tensile normal stress of a substrate!). Similarly, the ultimate shear strength of the NiO–Pt interfaces reported by Shieu et al. [34] to be as high as 4460 MPa for a Pt substrate with a tensile strength of 145 MPa is also rather doubtful. Using Eq. (9), Chen et al. [35] obtained the interfacial shear strength of a TiN coating on a steel substrate to be 650 MPa, which is also clearly higher than the shear flow strength of the steel (450 MPa). The analytical results on the interfacial shear stress distribution given by Jeong and Kwon [17] seem to have the characteristics somewhat similar to those obtained from our finite element analyses. Their equation used to compute the maximum interfacial shear strength is nevertheless still questionable. For a DLC thin coating on a soft annealed AA1050 substrate, the interfacial shear strength of the coating was reported to be 400–700 MPa by Jeong and Kwon [17], again well exceeding the maximum shear flow stress level of the substrate. Surprisingly, the analytical results given by Agrawal and Raj [16] and Jeong and Kwon [17] for estimating the interfacial shear strength of the coating do not require the knowledge on the plastic deformation properties of the substrate at all. As the fragmented coating can only be loaded by the substrate, the maximum shear stress that a ductile metal substrate can exert on the coating has to be limited by its plastic flow strength in *shear* at large strains. So their analytical results for estimating the interfacial shear strength of thin film coatings is invalid.

If indeed the interfacial shear strength of a coating is very high and it exceeds the maximum shear flow stress level of the substrate, then decohesion usually cannot be realized right at the coating–substrate interface. Instead, the substrate will have to deform at the cracked locations by growing either blunt notches or cracks into the substrate itself or by subsurface plastic deformation just below the interface. In either case, one can no longer assume that the strain in the fragmented coating is the same as the overall axial strain in the substrate (far from the coating region), as Jeong and Kwon [17] and Wang et al. [30] apparently did. Direct measurements of the strains in the coating is highly desirable and one should also observe carefully the crack opening characteristics while the coating–substrate remains loaded in tension (see Section 2) to distinguish the two possible deformation modes (coating decohesion vs. substrate damage, see Fig. 8). As coating decohesion was evident based on the microscopy images for our Al_2O_3/Al–5%Mg system, the finite element analysis was carried out only for the decohesion mode of the deformation in this study.

In summary, a brittle thin film deposited on the ductile substrate cracks under uniaxial tension once the accumulated shear stress transferred by the interface makes the tensile stress in the coating reach the fracture strength level. At relatively larger strains, decohesion of

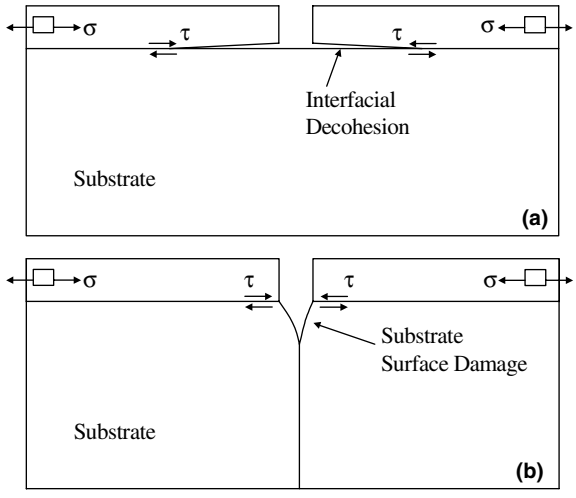

Fig. 8. Schematic of the two possible deformation modes after the through thickness cracking of a coating on a ductile substrate: (a) weak interface/strong substrate, decohesion along the interface; (b) strong interface/weak substrate, surface damage and fracture into the substrate.

the coating from the substrate may occur. While simple shear-lag type analyses [6,16,17] are valuable in understanding the coating fracture behavior *qualitatively*, the application of their analytical results such as Eq. (9) in *quantitatively* estimating the interfacial shear strength of a coating–substrate system is very questionable. Reliable measurements of the coating and coating–substrate interface properties by utilizing the uniaxial tensile test data require both a complete characterization of the plastic stress–strain response of the substrate at large strains and a more accurate stress analysis of the coating bonded to the substrate by the nonlinear finite element method. Our results presented here demonstrate that a proper selection of the interface parameters in the cohesive interface model used in the finite element analysis can provide consistent results of stress distributions in a ''unit cell'' single cracked segment and it leads to a more reliable means of measuring the fracture strength of the coating as well as the ultimate shear strength of the coating–substrate interface. If decohesion of the coating is completely absent, then the maximum shear flow stress level of the substrate can only serve as a lower bound estimate on the ultimate shear strength of the interface. One simply cannot at all use the uniaxial tension test to measure the interfacial shear strength of a coating that is higher than the maximum shear flow stress level of the substrate, as claimed in [16,17,33–35].

Acknowledgements

The authors acknowledge the assistance of Dr. L.G. Hector, Dr. H. Weiland, Dr. L.F. Wiserman with the preparation and testing of the anodic oxide coatings on aluminum substrates. The work reported was supported in part by the NSF Grant No. CTS-9871885 (Program Director: M. Roco).

References

[1] Keller F, Hunter MS, Robinson DL. J Electrochem Soc 1953;100:110.
[2] Edeleanu C, Law TJ. Phil Mag 1962;7:573.
[3] Bradhurst DM, Leach JSL. J Electrochem Soc 1966;113:1245.
[4] Grosskerutz JC, McNeil MB. J Appl Phys 1969;40:355.
[5] Hockenhull BS, Gupta SS, Hurst RC. Trans Inst Metal Finish 1976;54:123.
[6] Hu MS, Evans AG. Acta Metall 1989;37:917.
[7] Hutchinson JW, Suo Z. Mixed mode cracking in layered materials. Advances in applied mechanics, vol. 29. San Diego: Academic Press; 1992. p. 63.
[8] Ye T, Suo Z, Evans AG. Int J Solid Struct 1992;29:2639.
[9] Dauskardt RH, Lane M, Ma Q, Krishna N. Eng Fract Mech 1998;61:141.
[10] Müler D, Fromm E. Thin Solid Film 1995;270:411.
[11] Yang QD, Thouless MD, Ward SM. J Mech Phys Solid 1999;47:1337.
[12] Chechenin NG, Bottiger J, Krog JP. Thin Solid Film 1995;261:219.
[13] Kriese MD, Boismier DA, Moody NR, Gerberich WW. Eng Fract Mech 1998;61:1.
[14] Pang M, Wilson DE, Bahr DF. Mater Res Soc Symp Proc 2000;594:501.
[15] Abdul-Baqi A, Van Der Giessen E. Thin Solid Film 2001;381:143.
[16] Agrawal DC, Raj R. Acta Metall 1989;37:1265.
[17] Jeong JH, Kwon D. J Adhesion Sci Technol 1998;12:29.
[18] Tong W, Hector LG, Weiland H, Wiserman LF. Unpublished work; 1997.
[19] Xie C, Li X, Tong W, Hector LG, Weiland H, Wieserman LF. In: Proceedings of the SEM IX international congress on experimental mechanics, Orlando, FL; 2000. p. 16.
[20] Cairns DR, Sachsman SM, Sparacin DK, Witte II RR, Crawford GP, Paine DC. Mater Res Soc Symp Proc 2000;594:401.
[21] Delannay F, Warren P. Acta Metall Mater 1991;39:1061.
[22] Needleman A. Int J Fract 1990;42:21.
[23] Baney JM, Hui CY. J Adhesion Sci Technol 1997;11:393.
[24] Tvergaard V. Eng Frac Mech 2003;70:1859.
[25] Tong W. Exp Mech 1997;37:452.
[26] Tong W, Hector LG, Weiland H, Wiserman LF. Scripta Mater 1997;36:1339.
[27] Tong W. J Mech Phys Solid 1998;46:2087.
[28] Hertzberg RW. Deformation and fracture mechanics of engineering materials. 4th ed.. New York: Wiley; 1995.
[29] Beuth JL, Klingbeil NW. J Mech Phys Solid 1996;44:1411.
[30] Wang JS, Sugimura Y, Evans AG, Tredway WK. Thin Solid Films 1998;325:163.
[31] Cotterell B, Chen Z. Int J Fract 2000;104:169.
[32] Yu H, Hutchinson JW. Int J Fract 2002;113:39.
[33] Agrawal DC, Raj R. Mater Sci Eng A 1990;126:125.
[34] Shieu FS, Raj R, Sass SL. Acta Metall Mater 1990;38:2215.
[35] Chen BF, Hwang J, Yu GP, Hunag JH. Thin Solid Film 1999;352:173.